Colloids and Surfaces A: Physicochemical and Engineering Aspects 637 (2022) 128268

Contents lists available at ScienceDirect

Colloids and Surfaces A: Physicochemical and Engineering Aspects

journal homepage: www.elsevier.com/locate/colsurfa

Understanding drop spreading behaviour on WC-10wt%Co cutting tools – an experimental and numerical study

B. Guimarães [a,*], J. Silva [a], C.M. Fernandes [b], D. Figueiredo [b], O. Carvalho [a], G. Miranda [c,1], F. S. Silva [a,1]

[a] Center for MicroElectroMechanical Systems (CMEMS-UMinho), University of Minho, Campus de Azurém, 4800–058 Guimarães, Portugal
[b] Palbit S.A., P.O. Box 4, 3854–908 Branca, Portugal
[c] CICECO, Aveiro Institute of Materials, Department of Materials and Ceramic Engineering, University of Aveiro, 3810–193 Aveiro, Portugal

HIGHLIGHTS

- Contact angle of 75.3° for machining cutting fluid and 92.8° for distilled water.
- Drop spreading behaviour of both fluids on WC-10wt%Co evaluated by level set method.
- Results showed a good agreement between the numerical and experimental drop shape.
- Exponential dependency with a spreading factor of approximately $t^{1/2}$.
- Initial spreading stage controlled by balance between inertial and capillary forces.

GRAPHICAL ABSTRACT

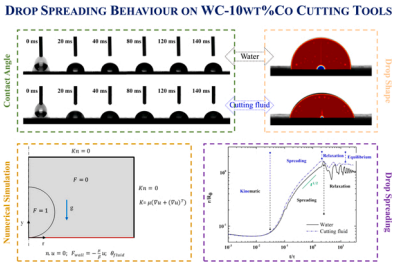

ARTICLE INFO

Keywords:
WC-Co cutting tools
Wettability
Level set method
Drop spreading
Spreading factor

ABSTRACT

WC-Co cutting tools performance under demanding cutting conditions largely depend on the efficiency of the cutting fluid, mainly its ability to remove heat and reduce friction, both highly dependent on the wettability and drop spreading behaviour of the fluid. In this context, this study focuses on the spreading behaviour of machining cutting fluid and water in WC-10 wt%Co cutting tools surface. Contact angles were experimentally measured and then used for performing numerical simulations by the level set method. A contact angle of 75.3° and 92.8° were measured for the machining cutting fluid and distilled water, respectively, and coincident values were found by numerical simulation, as well as a strong agreement in the drop shape. It was also possible to observe that machining cutting fluid has a lower spreading time than water, due to a lower contact angle and higher viscous dissipation, allowing to reach equilibrium phase sooner. Also, the machining cutting fluid presents a higher drop radius than water, meaning a 24.2% contact area increase over 50 ms of spreading time. Furthermore, numerical simulation showed that the drops spreading over the capillary-inertial time, at the early stage of spreading, follow an exponential dependency with a spreading factor of approximately $t^{1/2}$, which indicates that the initial spreading of both drops is driven and controlled by the balance between inertial and capillary forces. This work intends to contribute to the knowledge on the phenomena that drive the drop spreading behaviour on WC-10 wt%Co cutting tools, being the development of numerical models to predict this behaviour of utmost importance, since it can lead to the development of novel surface improved tools, with an enhanced lubrification effect and

* Corresponding author.
E-mail addresses: brunopereiraguimaraes@hotmail.com, bguimaraes@dem.uminho.pt (B. Guimarães).
[1] Co-last authorship

https://doi.org/10.1016/j.colsurfa.2022.128268
Received 20 September 2021; Received in revised form 12 December 2021; Accepted 3 January 2022
Available online 5 January 2022
0927-7757/© 2022 The Authors. Published by Elsevier B.V. This is an open access article under the CC BY-NC-ND license (http://creativecommons.org/licenses/by-nc-nd/4.0/).

heat removal capacity closer to the cutting zone during machining processes, and consequently allowing an improvement in the tribological and cutting performance of these tools.

Nomenclature

WC	Tungsten Carbide
Co	Cobalt
r	Radius of wetted area (m)
t	Time (s)
Ra	Arithmetic average surface roughness (μm)
u	Fluid velocity (m/s)
γ	Reinitialization parameter
ϵ	Thickness of the interface between the two fluids (m)
F	Level set function
ρ	Density (kg/m^3)
μ	Dynamic viscosity (Pa.s)
g	Gravitational acceleration (m/s^2)
$F\sigma$	Force due to surface tension (N/m^3)
σ	Surface tension (N/m)
I	Identity matrix
n_{int}	Interface normal
δ	Dirac delta function associated to the interface
Kn	Viscous stress
β	Slip length (m)
θ	Contact angle ()
$r/R0$	Spreading factor
τ	Capillary-inertial time (s)
α	Exponent value
C	Coefficient
We	Weber number – $\rho u^2 D/\sigma$
Re	Reynolds number – $\rho u D/\mu$
D	Drop diameter before impact (m)

1. Introduction

Spreading of a liquid drop over solid surfaces is an interesting phenomenon from both fundamental and applied viewpoints, often encountered in several fields of science and engineering, and playing an important role in several industrial applications, such as rain drops on automobile windshields, inkjet and metal deposition in manufacturing processes, internal combustion engines, spray cooling of electronics, spray coating and painting for various applications, and lubrication/cooling in machining processes [1–3].

Despite its apparent simplicity, the behaviour of a drop spreading on a solid surface is a very complex problem, that has been described by Rioboo et al. [4] as a sequence of four successive phases: kinematic, spreading, relaxation and wetting/equilibrium. Indeed, the wetting of a solid by a liquid concerns scales from the capillary length to the Van der Waals forces and remains only partially understood due to the intricate interaction between droplet and surface [5,6]. When a liquid drop contacts a wettable surface, the liquid spreads over to minimize the total surface energy, being the first instants of spreading very fast (some milliseconds for millimeter sized water drops), while it takes a much longer time for viscous liquids to completely spread [7]. The important factors governing the drop dynamics on a solid surface are the liquid properties (surface tension, viscosity and density), the surface characteristics (roughness and contact angle), the drop size and impact velocity, the surface inclination and the surrounding pressure [8,9], as shown in the experimental investigations performed by Šikalo et al. [10–12] with liquids of different surface tensions and viscosities (e.g., isopropanol, water and glycerin), where the drop volume, surface inclination and impact velocity had a significant effect on the drop dynamics and regimes of drop impact.

The wetting behaviour of liquids on a surface depends on which forces are resisting to deformation and, generally, follows an exponential law, where the value of the exponent depends on inertia, viscosity and surface wettability [7,13,14]. The most popular exponential law, which relates the radius of the wetted area (r) with time (t) is the Tanner's law (Eq. 1), with $n = 1/10$ [15–17].

$$r\ (t) \sim t^n \tag{1}$$

Tanner's law is suitable to predict spreading behaviours in which surface tension is balanced by viscosity. Depending on the different contributions of viscosity, surface tension, inertia and gravity, different evolutions have been reported: $n = 0.1$, $n = 0.14$, $n = 0.16$, $n = 1/8$, $n = 1/7$, $n = 1/2$ [7,17]. For the early stage of spreading, particularly for low viscosity fluids, such as water, it is well known that the growth of droplets diameter, upon wetting, follows a power law with an exponent of approximately 1/2, due to the balance between inertial and capillary pressure [13,15].

In addition to experimental investigations, several numerical studies on the spreading of a liquid drop over solid surfaces have been reported in literature, being different numerical methods available for evaluating the evolution of the fluid interface, along with ways to implement moving contact line models (see [18] for a detailed review article on this subject). For example, the level set method, originally proposed by Osher and Sethian [19], is an implicit method to capture the moving front. The basic idea is that the front location is given as the zero level set of an auxiliary field defined over the domain of interest. This method was used by Cheng et al. [20] to develop a transient two-dimensional axisymmetric model for numerical investigation of drop spreading and heat transfer on hot substrates that was validated with experimental data. It was found that the predicted drop spreading radius agrees quite well with the experimental data and that the drop spreading rate will increase with increasing impact velocity, surface tension and initial radius, or decreasing equilibrium contact angle and liquid viscosity. Zhang and Yue [21] developed a level-set method in the finite-element framework, being the predicted contact line dynamics able to match the Cox theory very well. Furthermore, their method can be easily modified to compute contact angle hysteresis. Hashemi et al. [22] simulated the spreading of droplets in contact with solid substrates on three-dimensional computational domains and compared the results with experimental data in order to validate the model. Other method, the volume of fluid method, which uses the volume fraction of the traced fluid to track the interface position was employed by Russo et al. [23] to develop a numerical model capable of accurately simulate the drop impact on spatially nonuniform wettability patterns of any foreseeable design. Seksinsky and Marshall [24] combined the level-set volume of fluid method for droplet impingement on a flat surface at low drop Reynolds numbers and validated the computational predictions with existing experimental data. Results showed that the surface area over which the drop spreads increase with the increase in Reynolds number. Shang et al. [25] proposed a three-dimensional front tracking method that integrates the generalized Navier boundary condition to model the moving contact line of droplets on a solid surface. This method employs a discrete set of linked Lagrangian markers to represent the interface and

the contact line position is updated according to either the fluid velocity at the contact line or the contact angle. The simulation of a sessile drop showed good agreement with the analytic solution, with errors of less than 0.4%, and a numerical convergence test indicated convergence of the surface tension calculation and the contact line model. The front tracking method was also used by Muradoglu and Tasoglu [26] to evaluate the impact and spreading of glycerin droplets on wax and glass substrates, being the numerical results in a good agreement with the experimental data. Finally, the diffuse interface method can also be used to evaluate the spreading of a liquid drop over solid surfaces. Shahmardi et al. [27] employed this method to propose a fully Eulerian hybrid immersed-boundary phase-field model for simulating contact line dynamics on any arbitrary geometry, being the suggested algorithm capable of modelling both static and dynamic contact angle boundary conditions with possibly slip velocity at the wall. The numerical tests reported in this study validate the algorithm against different results from the literature on wetting and two-fluid systems. Liu et al. [28] investigated the maximal spreading ratio of an impacting compound drop at moderate Reynolds and Weber numbers on a hydrophobic substrate by using a ternary-fluid diffuse-interface method. The maximal spreading ratio of the compound drop was found to depend on the volume fraction of the inner drop, the surface tension ratio, the Weber number and the flow regime.

Machining cutting fluids have been widely used in industry to achieve longer tool life and greater dimensional accuracy, through the high cooling capacity and enhanced lubricating ability of the fluid, that allows to dissipate about 96% of heat generated in the workpiece and cutting tool by forced convection [29,30]. The use of machining cutting fluids helps reducing machining costs in four ways [31]: first, reduce the cost of the tool as a direct result of reducing tool wear; second, increase production rates, since higher machining speeds can be achieved when using cutting fluids; third, the use of fluids reduces labour cost indirectly, by eliminating downtimes; finally, reduces energy consumption as a result of reducing the frictional forces between the tool and chips, and the tool and workpiece by lubricating these surfaces. In addition to these, there are other less important roles for machining fluids, such as facilitating chip removal and rust protection for the workpiece, cutting tool, and machine [30].

In this sense, the understanding of drop spreading over cemented carbide surfaces, namely WC-Co (the most commonly used material for cutting tools due to the inherent high hardness and toughness, and wear resistance [32–34]), and consequent ability to enhance theses surfaces wettability is undoubtedly valuable, since a good surface wettability is beneficial for the tribological and cutting performance of these tools [35,36]. Yin et al. [37] studied the physiochemical properties and the lubrification effect of six base oils in MQL milling of AISI 1045. It was found that the contact angle decreases with the decrease in surface tension and that a large wetting area decreases surface roughness of the workpiece and milling force, as well as leading to an improvement in the workpiece surface quality. Wang et al. [38] simulated the spreading and wetting behaviour of microdroplets in a textured tool surface with controllable structure and conducted turning experiments of the tools with six different textures in aluminium alloy 6061-T6. Results showed that the texture can change the spreading state on the tool surface, and the lubricating fluid can effectively enter in the texture and tend to flow along the direction of the groove.

The aim of this work was to evaluate experimental and numerically the early-stage drop spreading behaviour of two different fluids, water and machining cutting fluid, on WC-Co cutting tools surface in order to better understand this phenomenon. The time evolution of the spreading radius, *r(t)*, was analysed, as well as the time for the complete spreading of the drop and discussed with the results found in the literature. The shape of the drop simulated by the level set method was also compared with the experimental measurements.

2. Experimental work

In this study, WC-10 wt%Co substrates with an arithmetic average roughness (Ra) of 0.69 ± 0.13 μm were used for wettability evaluation of two different fluids, distilled water and machining cutting fluid (5% volume concentration). These substrates were produced by Palbit S.A., being the microstructure presented in Fig. 1. Roughness measurements were performed with Mitutoyo Surftest SJ-210 portable surface roughness tester, using surface ISO 1997 standard, with a diamond tip radius of 2 μm and 60° angle. A total length of 1.25 mm was used for the measurement, being 1.00 mm of evaluation length and a cut-off of 0.25 mm with a measurement speed of 0.25 mm/s. A total of 10 measurements were made for each sample.

Before performing the wettability measurements, the WC-Co substrates were ultrasonically cleaned for 2 min in ethanol. The contact angles were studied by sessile drop method using an optical tensiometer (OCA 15 plus, Dataphysics, Germany), at room temperature (≈ 20 °C), using 5 μL of fluid dispensed by a micrometric syringe. The determination of contact angles was done with DataPhysics SCA—software using the Laplace–Young's method, after fitting drop outline to the recorded images. For these measurements, five contact angle readings were made for each fluid at 140 ms (necessary time for drop stabilization) and the behaviour of the drop was video recorded with a frame rate of 50 frames per second at a resolution of 768 × 576 pixels.

For numerical simulation purposes, the surface tension and dynamic viscosity of machining cutting fluid were assessed at room temperature (≈ 20 °C) and are presented in Table 1. Surface tension was determined by pendant drop method with the same equipment used for wettability measurements and dynamic viscosity was measured with a Brookfield STS-2011 rotational viscometer at a shear rate of 132 s^{-1} with a TL5 turning spindle for a sample volume of 6.7 ml.

3. Numerical simulation

3.1. Mathematical model and fluids properties

For the numerical simulations performed in this study, COMSOL Multiphysics software was used to evaluate the spreading behaviour of water and machining cutting fluid drops over a period of time. To track the position of the interface (free surface) between two immiscible fluids, in this case water and air, and machining cutting fluid and air, a level set method was used. Thereby, the governing equation is presented in Eq. (2).

$$\frac{\partial F}{\partial t} + u.\nabla F = \gamma\nabla.\left(\varepsilon\nabla F - F(1-F)\frac{\nabla F}{|\nabla F|}\right) \quad (2)$$

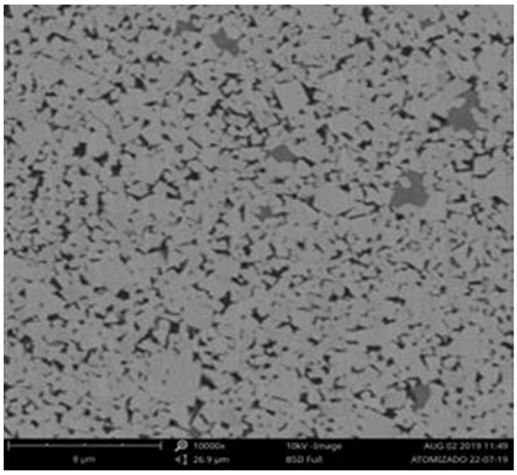

Fig. 1. WC-10 wt%Co substrates microstructure.

Table 1
Properties of water, machining cutting fluid and air at 20 ℃.

Property	Symbol	Fluid	Value
Dynamic viscosity	μ	water	1.002×10^{-3} Pa.s[40]
		cutting fluid	1.566×10^{-3} Pa.s
		air	1.825×10^{-5} Pa.s[41]
Density	ρ	water	998.2 kg/m^3[40]
		cutting fluid	975 kg/m^3
		air	1.204 kg/m^3[41]
Surface Tension	σ	water/air	0.0728 N/m[40]
		cutting fluid/air	0.0441 N/m

In this equation, u (m/s) represents the velocity field, γ (m/s) the reinitialization parameter and ϵ (m) the thickness of the interface between the two fluids, which is taken as half of the length of the mesh element. The level set function, F, is a scalar function which sets the interface shape of the element. If F is equal to 1 the elements which discretize the domain are set to fluid, while if F is 0 the corresponding region of the domain is set to be occupied by air. Only at the interface between the two fluids, the level set function varies smoothly from 0 to 1 [39].

Since there is no remesh, the properties of the domains are dependent of the value of the level set function. Therefore, the density, ρ (kg/m^3), and the dynamic viscosity, μ (Pa.s), are computed by Eqs. (3 and 4), respectively. The properties of water, machining cutting fluid and air are summarized in Table 1.

$$\rho = \rho_{air} + (\rho_{fluid} - \rho_{air})F \tag{3}$$

$$\mu = \mu_{air} + (\mu_{fluid} - \mu_{air})F \tag{4}$$

To compute mass and momentum conservation, COMSOL Multiphysics software was also used. The fluids are assumed to be Newtonian and incompressible with no phase change. Under isothermal condition and in the absence of any surfactant, the surface tension is constant and uniform at the interface between the two fluids. In such conditions, the velocity field u and the pressure P satisfy the classical one-fluid formulation of the Navier–Stokes equations [7]:

$$\nabla . u = 0 \tag{5}$$

$$\rho\left(\frac{\partial u}{\partial t} + u.\nabla u\right) = -\nabla P + \nabla.\left(\mu\left(\nabla u + (\nabla u)^T\right)\right) + \rho g + F_\sigma \tag{6}$$

In Eq. (5), the mass conservation is obtained by setting the divergence of the velocity field as zero and the momentum conservation, describing the balance of forces acting on the fluid, is expressed by Eq. (6), where g (m/s^2) is the gravitational acceleration and F_σ (N/m^3) the force due to surface tension, which is computed according to Eq. (7):

$$F_\sigma = \nabla.\left(\sigma\left(I - \left(n_{int}n_{int}^T\right)\right)\delta\right) \tag{7}$$

where σ (N/m) represents the surface tension, I the identity matrix, n_{int} the interface normal and δ the Dirac delta function associated to the interface, that is nonzero only at the interface between the two fluids [39].

3.2. Geometrical definition and boundary conditions

The simulation was performed considering an axial-symmetry of the fluid drop and air domain. Therefore, in Fig. 2 is illustrated half of a fluid drop, which radius is approximately 1.06 mm (5 μL volume), and the surrounding air at the initial state.

Fig. 2 also represents the boundary conditions used in the numerical model. It is imposed an open boundary condition on the outside boundaries of the air domain, to describe that these boundaries are in contact with a large volume of fluid [39], setting the vanishing of viscous stress ($Kn = 0$) [42]. The bottom boundary is set as a wetted wall

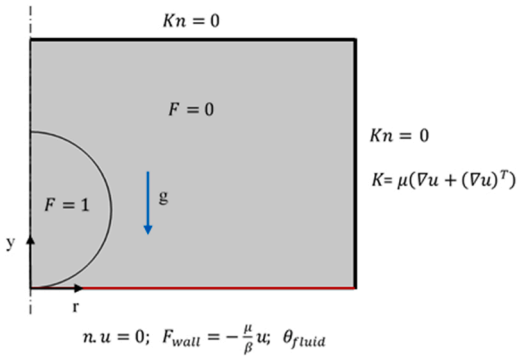

Fig. 2. Geometrical representation of the model and its boundary conditions at initial state.

boundary condition. This condition does not let the fluid flow through the boundary, by setting the normal component of velocity field as zero. Also, at this boundary, a Navier Slip boundary condition is added, which is a frictional force, where μ represents the fluid viscosity, β (m) the slip length, which is taken as the mesh element size, and u the fluid velocity field. The last boundary condition, set at this boundary, is the equilibrium contact angle, which adds a force due to the surface tension contribution at the wall. In addition, in Fig. 2, is also illustrated the initial conditions for the level set function, where the fluid drop is defined with a scalar value of 1 and its surrounding domain as 0 (air). The initial velocity field is also set as zero for all the domains.

The domains are discretized with triangular elements only, with a maximum element size of 31.80 μm, which resulted in a total of 38388 elements. Regarding skewness parameter, as a measure of elements quality, this has an average value of 0.94, for all the domains, and a minimum value of 0.57. This parameter indicates how close the elements are from their ideal shape, being the higher quality obtained for skewness values closer to 1.

4. Results and discussion

4.1. Experimental results

The results obtained from sessile drop measurements with distilled water and machining cutting fluid are presented in Fig. 3a) and b), respectively. Due to uncertainty associated with the frame rate of the video recorded, it was established that the contact time (t = 0 ms) corresponds to the first frame where any visual changes are observed. In this sense, the spreading behaviour was evaluated until 140 ms of spreading time was achieved.

A contact angle of $92.8^\circ \pm 2.6^\circ$ and $75.3^\circ \pm 2.3^\circ$ was measured for distilled water and machining cutting fluid, respectively, at t = 140 ms (Fig. 3) of spreading time, allowing to conclude that the cutting fluid presents a higher wettability for the WC-10 wt%Co substrates, being this behaviour in accordance with literature [43]. These contact angle values were then used in the numerical simulation. In Fig. 3, it is possible to notice that the drop spreading is a very fast phenomenon, being needed

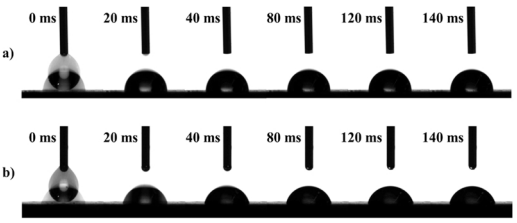

Fig. 3. Contact angle evolution of the WC-10 wt%Co substrates: a) distilled water and b) machining cutting fluid.

only around 20 ms to achieve a drop shape similar to the one in equilibrium state. It is also possible to notice that the machining cutting fluid drop reaches equilibrium faster than the distilled water drop. These observations are in strong agreement with the numerical simulations performed in this study and with the literature, since it is reported that the spreading time (i.e. the necessary time to achieve equilibrium phase) increases with the increase in contact angle [7,13,44].

4.2. Numerical simulation results

The numerical simulation was performed, for both fluids, until 140 ms of drop spreading was reached. Fig. 4 illustrates the evolution of spreading behaviour of the machining cutting fluid drop shape ($\theta = 75.3^{\circ}$) for several time steps, where the colour legend is related to the level set function, which sets which fluid occupies each mesh element. The time steps are non-regular, in order to show particular events observed during spreading.

Initially, when the cutting fluid drop touches the wall, the formation of a "neck" occurs (t = 1.23 ms). Then, the top of the drop starts moving due to the appearance of a capillary wave induced by the initial impulse generated at the contact line, causing an elevation of the top of the drop until a maximum drop height of approximately 2.50 mm at t = 6.56 ms, which is 18.13% more than the initial drop diameter, as shown in Fig. 5a). This behaviour is in accordance with numerical simulations previously reported in literature [7,45]. Consequently, combined with the displacement of the contact line, the drop is elongated into two orthogonal directions, resulting in the generation of a pinch event (t = 9.73 ms), that leads to a maximum spreading radius of approximately 1.74 mm, 63.98% more than the initial drop radius, at t = 11.25 ms, as depicted in Fig. 5b). Due to the capillary wave originated by the coalescence of the pinch event, a second pinch event is formed at t = 12.10 ms. These pinch events are responsible for the contact line oscillations shown in Fig. 7, at both early and final stage of spreading [46]. Between t = 80 ms and t = 140 ms the spreading radius variations are negligible, being differences in the drop shape hardly identifiable, as it can be visualized in Fig. 4 and confirmed by the experimental results depicted in Fig. 3.

The spreading behaviour evolution for the water drop shape with a contact angle of 92.8° is illustrated, for several time steps, in Fig. 6. Once again, the time steps are non-regular, in order to show particular events observed during spreading.

Similarly, to the spreading behaviour of cutting fluid, the water drop forms a "neck" when the drop touches the wall (t = 1.20 ms). Then, the top of the drop starts moving due to the appearance of a capillary wave induced by the initial impulse generated at the contact line, leading to a maximum drop height of approximately 2.40 mm at t = 5.04 ms, which is 13.15% more than the initial drop diameter, as shown in Fig. 5a). Therefore, combined with the displacement of the contact line, the drop is elongated into two orthogonal directions until it reaches the maximum spreading radius of approximately 1.71 mm, 61.16% more than the initial drop radius, at t = 10.08 ms (see Fig. 5b). It is also possible to notice that due to the presence of capillary waves, more oscillations in the drop shape occur than in comparison with the drop shape evolution for machining cutting fluid.

Fig. 5 depicts the drop height and radius evolution for water and machining cutting fluid over 50 ms of spreading time. It is possible to observe that the cutting fluid drop achieve its maximum drop height and radius at a later spreading time than water. This phenomenon can be explained by the lower surface tension of the machining cutting fluid. As it is known, the Weber number determines the maximum diameter of the drop, so as it increases it takes longer to achieve the maximum drop height and consequently maximum drop radius, because the initial impulse transmitted to the drop is decreased [3,47]. Also, the machining cutting fluid presents a higher drop radius than water, meaning a 24.2% contact area increase over 50 ms of spreading time, since a small contact angle increases the wetting area, which leads to an enhanced

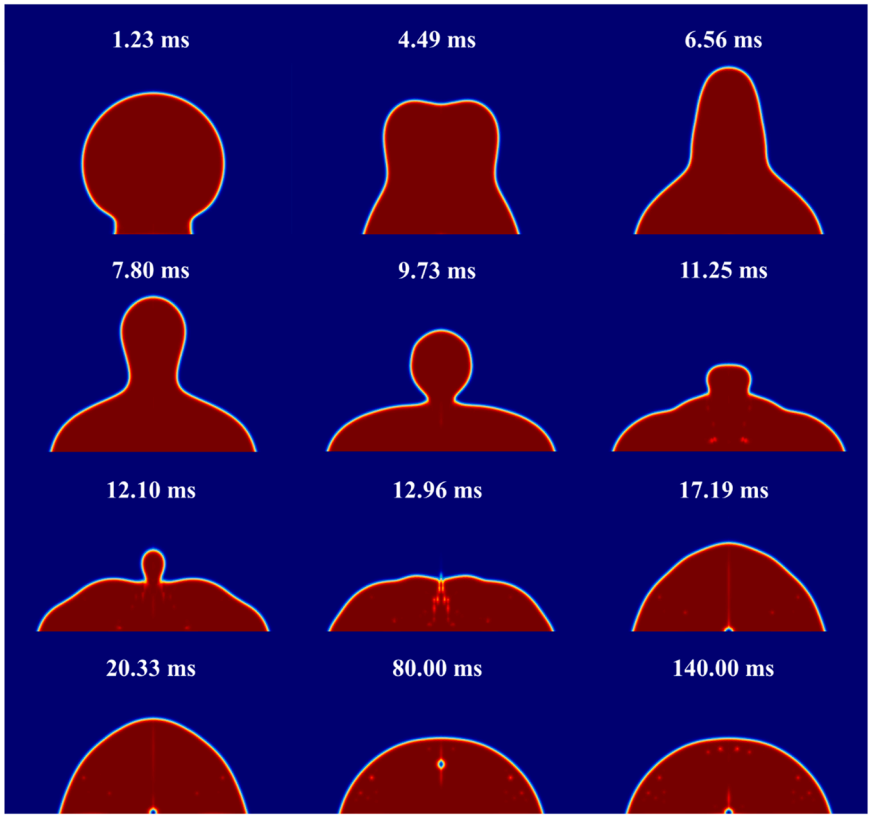

Fig. 4. Spreading behaviour evolution of a machining cutting fluid drop on a surface with a contact angle of 75.3° for several time steps.

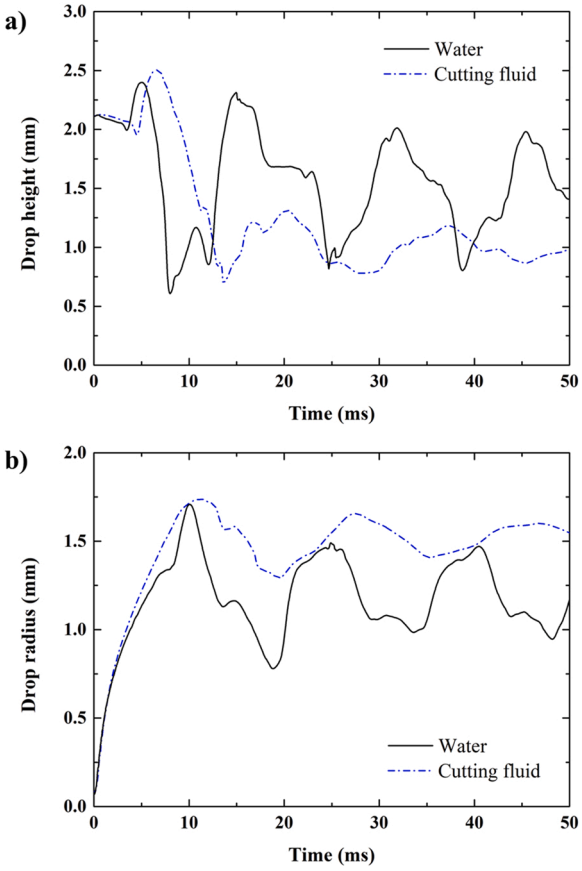

Fig. 5. a) drop height and b) drop radius evolution for water and machining cutting fluid over 50 ms of spreading time.

lubrification effect and heat removal capacity during machining processes, and consequently allowing an improvement in the tribological and cutting performance of WC-Co cutting tools [37,48,49].

One parameter that is very important in drop dynamics is the spreading factor (r/R_0), that is usually given by the ratio between the radius of the drop at a determined moment of time and the initial drop radius. Looking more closely to the initial stage of spreading, the growth of the spreading factor collapses into an approximately $t^{1/2}$ exponential law (see Fig. 7), indicating that the initial spreading behaviour of the fluids studied in this work is driven and controlled by a balance between inertial and capillary forces, which is in accordance with results reported in literature [4,7,15]. In Fig. 7, the spreading factor log-log plot is presented as function of time normalized by the capillary-inertial time (τ). Therefore, the spreading factor over time can be approximated by Eq. (8), where α is the exponent value, C is a coefficient, and the capillary-inertial time can be calculated by Eq. (9).

$$\frac{r}{R_0} = C\left(\frac{t}{\tau}\right)^{\alpha} \tag{8}$$

$$\tau = \sqrt{\frac{\rho \quad R_0^3}{\sigma}} \tag{9}$$

An exponent value of 0.539 and 0.503 was obtained for cutting fluid and water, respectively, while the coefficient C is approximately 1.161 and 0.968, respectively. These results are very satisfactory for both cases and are in agreement with literature, where it is reported that α and C decrease with the increase in contact angle [13].

As seen in Fig. 7, wetting has a significant effect on the spreading rate. From literature, it is expected an increase in spreading time when increasing the contact angle [7,44]. Indeed, the spreading factor curve of water is more shifted to the right, meaning that the spreading time increases, since it presents a higher contact angle than the machining cutting fluid. Also, in Fig. 7, the four different stages of drop dynamics are observable. In the kinematic phase, the spreading factor remains practically unaltered and both fluids present the same behaviour, being the differences between them negligible. This phase ends when the drop starts moving radially and mainly not vertically. As the spreading phase begins, other parameters such as the diameter of impacting drop, velocity, surface tension, density and viscosity start to influence the spreading process. During the later stage of this phase, surface tension plays a prominent role in undermining the maximum spread that the drop can achieve. After spreading to its maximum radius, the drop enters in the relaxation stage, where it may start receding (in this case several relaxation cycles occur for both fluids) before reaching the equilibrium phase [3,4,9]. It is important to notice that for the water drop, the relaxation time lasts until the end of the evaluated time (140 ms) and the spreading factor variations are higher and more frequent, allowing to conclude that the equilibrium phase may not yet been reached. This is due to the fact that Reynolds number is responsible for controlling the time it takes for the drop to reach equilibrium phase and, since the water has lower dynamic viscosity, which increases Reynolds number in comparison with cutting fluid leading to a higher necessary time to achieve the equilibrium phase due to a lower viscous dissipation [3,44].

Fig. 7 also allows to conclude, that the spreading factor features oscillations in the very initial stage of spreading and after reaching the maximum spreading factor. These oscillations are due to capillary waves, which travels from the contact line to the top of the fluid drop, as previously explained.

Beyond the analysis of the numerical results for the spreading behaviour, the drop shape of the fluids at t = 140 ms was also analysed. For this purpose, the shape of the numerical drops was compared with the shape of the experimental one measured by sessile drop method, as shown in Fig. 8. This comparison showed a good agreement between the numerical and experimental results with only a small difference found, that can be attributed to the error associated to the contact angle measurements. These results show that is possible to accurately predict the drop shape evolution for machining cutting fluid and water droplets, leading to a better comprehension of the spreading behaviour on WC-Co cutting tools surface.

5. Conclusions

In the present study, the level set method was used to perform numerical simulations in order to evaluate the spreading behaviour of two fluids, machining cutting fluid and water, on WC-10wt%Co surface. The contact angle used in the numerical simulations, was first experimentally measured by the sessile drop method. A contact angle of 75.3° and 92.8° were measured for the machining cutting fluid and distilled water, respectively, at t = 140 ms of spreading time, allowing to conclude that the cutting fluid presents a higher wettability. It was also possible to observe that the machining cutting fluid drop reaches equilibrium faster than the distilled water drop, being these observations in strong agreement with the numerical simulations results performed in this study and with the literature.

Numerical simulations showed that machining cutting fluid has a lower spreading time than water, due to lower contact angle and higher viscous dissipation, allowing to reach equilibrium phase sooner. Also, the machining cutting fluid presents a higher drop radius than water, meaning a 24.2% contact area increase over 50 ms of spreading time, which will lead to an enhanced lubrification effect and heat removal capacity during machining processes. Moreover, the drop spreading over the capillary-inertial time, at the early stage of spreading, showed an exponential dependency with a spreading factor of approximately $t^{1/2}$, more precisely 0.539 and 0.503 for cutting fluid and water, respectively. The approximation with this specific exponential law allows to conclude that the initial stage of spreading may be governed and

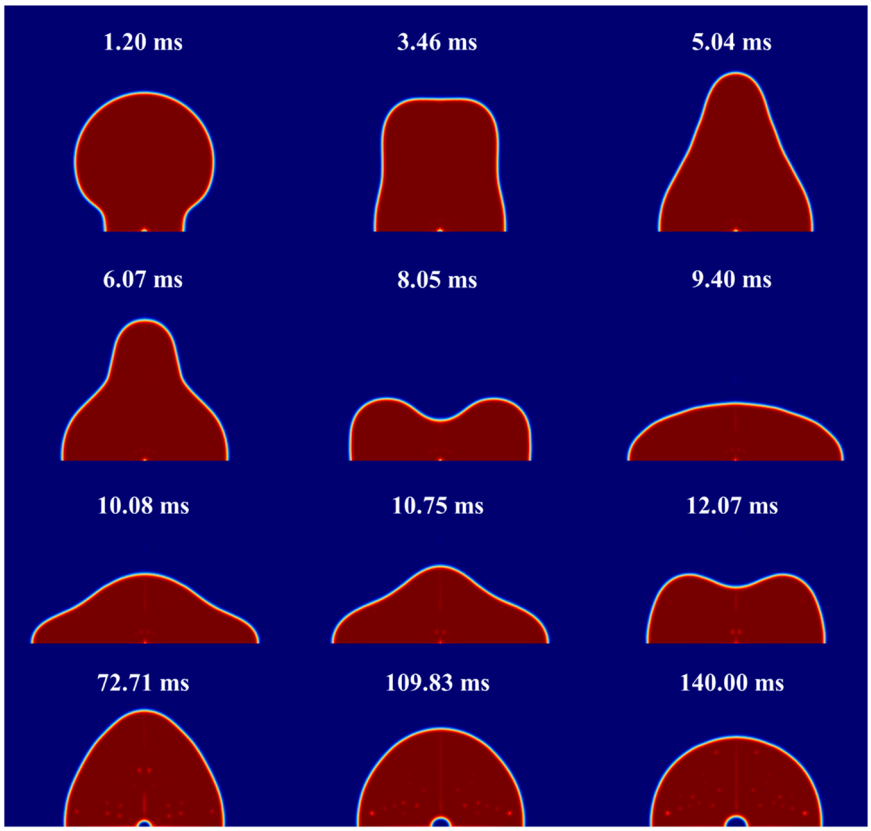

Fig. 6. Spreading behaviour evolution of a water drop on a surface with a contact angle of 92.8° for several time steps.

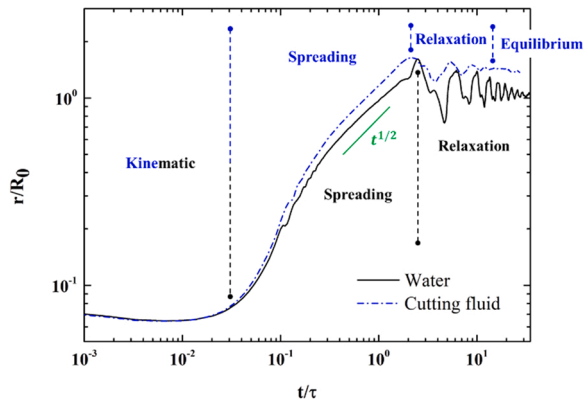

Fig. 7. Spreading factor as a function of the normalized capillary-inertial time, collapsing in an approximately $t^{1/2}$ exponential law. The four different phases of drop impact dynamics are also presented.

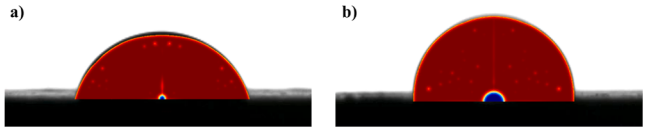

Fig. 8. Drop shape comparison between the numerical and experimental results of a) cutting fluid and b) water at 140 ms of spreading time.

controlled by the balance of inertial and capillary forces.

This study results show that is possible to accurately predict the drop shape evolution for machining cutting fluid and water droplets on WC-10wt%Co surface, being the numerical and experimental drop shape for both fluids in strong agreement. In this sense, this work allows to strengthen the basic understanding of drop spreading behaviour on WC-Co cutting tools, as well as predict the fluid behaviour depending on the physical properties, since it allows concluding that fluids with smaller contact angle have a larger spreading area, which will lead to an increased lubrification effect and ability to remove more heat and closer to the cutting zone, and consequently an enhancement in the tribological and cutting performance of these tools.

CRediT authorship contribution statement

B. Guimarães: Conceptualization, Methodology, Software, Investigation, Writing – original draft, Visualization. **J. Silva:** Methodology, Software, Investigation. **C. M. Fernandes:** Conceptualization, Resources, Writing – review & editing, Supervision. **D. Figueiredo:** Resources. **O. Carvalho:** Investigation. **G. Miranda:** Conceptualization, Writing – review & editing, Supervision. **F. S. Silva:** Writing – review & editing, Supervision.

Declaration of Competing Interest

The authors declare that they have no known competing financial interests or personal relationships that could have appeared to influence the work reported in this paper.

Acknowledgements

This work was supported by FCT (Fundação para a Ciência e a Tecnologia) through the grant 2020.07155.BD and by the project POCI-01–0145-FEDER-030353 (SMARTCUT). Additionally, this work was supported by FCT national funds, under the national support to R&D units grant, through the reference projects UIDB/04436/2020 and UIDP/04436/2020.

UMINHO CMEMS CENTER FOR MICROELECTROMECHANICAL SYSTEMS
REPÚBLICA PORTUGUESA CIÊNCIA, TECNOLOGIA E ENSINO SUPERIOR
FCT Fundação para a Ciência e a Tecnologia
NORTE2020 PROGRAMA OPERACIONAL REGIONAL DO NORTE
POCH PROGRAMA OPERACIONAL CAPITAL HUMANO
PORTUGAL 2020
UNIÃO EUROPEIA Fundo Social Europeu

References

[1] M. Reddy, M. Manivannan, M.G. Basavaraj, S.P. Thampi, Statics and dynamics of drops spreading on a liquid-liquid interface, Phys. Rev. Fluids 5 (2020), 104006, https://doi.org/10.1103/PhysRevFluids.5.104006.
[2] Q. Zhao, W. Ren, An energy-stable finite element method for the simulation of moving contact lines in two-phase flows, J. Comput. Phys. 417 (2020), 109582, https://doi.org/10.1016/j.jcp.2020.109582.
[3] A. Gupta, R. Kumar, Droplet impingement and breakup on a dry surface, Comput. Fluids 39 (2010) 1696–1703, https://doi.org/10.1016/j.compfluid.2010.06.006.
[4] R. Rioboo, M. Marengo, C. Tropea, Time evolution of liquid drop impact onto solid, dry surfaces, Exp. Fluids 33 (2002) 112–124, https://doi.org/10.1007/s00348-002-0431-x.
[5] P.G. De Gennes, Wetting: statics and dynamics, Rev. Mod. Phys. 57 (1985) 827–863, https://doi.org/10.1103/RevModPhys.57.827.
[6] J.B. Dupont, D. Legendre, Numerical simulation of static and sliding drop with contact angle hysteresis, J. Comput. Phys. 229 (2010) 2453–2478, https://doi.org/10.1016/j.jcp.2009.07.034.
[7] D. Legendre, M. Maglio, Numerical simulation of spreading drops, Colloids Surf. A Physicochem. Eng. Asp. 432 (2013) 29–37, https://doi.org/10.1016/j.colsurfa.2013.04.046.
[8] S.F. Lunkad, V.V. Buwa, K.D.P. Nigam, Numerical simulations of drop impact and spreading on horizontal and inclined surfaces, Chem. Eng. Sci. 62 (2007) 7214–7224, https://doi.org/10.1016/j.ces.2007.07.036.
[9] S. Jung, I.M. Hutchings, The impact and spreading of a small liquid drop on a non-porous substrate over an extended time scale, Soft Matter 8 (2012) 2686–2696, https://doi.org/10.1039/c2sm06565g.
[10] Š. Šikalo, M. Marengo, C. Tropea, E.N. Ganić, Analysis of impact of droplets on horizontal surfaces, Exp. Therm. Fluid Sci. 25 (2002) 503–510, https://doi.org/10.1016/S0894-1777(01)00109-1.
[11] Š. Šikalo, C. Tropea, E.N. Ganić, Impact of droplets onto inclined surfaces, J. Colloid Interface Sci. 286 (2005) 661–669, https://doi.org/10.1016/j.jcis.2005.01.050.
[12] Š. Šikalo, C. Tropea, E.N. Ganić, Dynamic wetting angle of a spreading droplet, Exp. Therm. Fluid Sci. 29 (2005) 795–802, https://doi.org/10.1016/j.expthermflusci.2005.03.006.
[13] J.C. Bird, S. Mandre, H.A. Stone, Short-time dynamics of partial wetting, Phys. Rev. Lett. 100 (2008), 234501, https://doi.org/10.1103/PhysRevLett.100.234501.
[14] L. Chen, E. Bonaccurso, M.E.R. Shanahan, Inertial to viscoelastic transition in early drop spreading on soft surfaces, Langmuir 29 (2013) 1893–1898, https://doi.org/10.1021/la3046862.
[15] K.G. Winkels, J.H. Weijs, A. Eddi, J.H. Snoeijer, Initial spreading of low-viscosity drops on partially wetting surfaces, Phys. Rev. E. 85 (2012), 055301, https://doi.org/10.1103/PhysRevE.85.055301.
[16] L. Tanner, The spreading of silicone oil drops on horizontal surfaces, J. Phys. D. Appl. Phys. 12 (1979) 1473–1484, https://doi.org/10.1088/0953-8984/2/S/067.
[17] D. Bonn, J. Eggers, J. Indekeu, J. Meunier, Wetting and spreading, Rev. Mod. Phys. 81 (2009) 739–805, https://doi.org/10.1103/RevModPhys.81.739.
[18] Y. Sui, H. Ding, P.D.M. Spelt, Numerical simulations of flows with moving contact lines, Annu. Rev. Fluid Mech. 46 (2014) 97–119, https://doi.org/10.1146/annurev-fluid-010313-141338.
[19] S. Osher, J.A. Sethian, Fronts propagating with curvature-dependent speed: algorithms based on Hamilton-Jacobi formulations, J. Comput. Phys. 79 (1988) 12–49, https://doi.org/10.1016/0021-9991(88)90002-2.
[20] Y. Cheng, F. Wang, J. Xu, D. Liu, Y. Sui, Numerical investigation of droplet spreading and heat transfer on hot substrates, Int. J. Heat. Mass Transf. 121 (2018) 402–411, https://doi.org/10.1016/j.ijheatmasstransfer.2018.01.026.
[21] J. Zhang, P. Yue, A level-set method for moving contact lines with contact angle hysteresis, J. Comput. Phys. 418 (2020), 109636, https://doi.org/10.1016/j.jcp.2020.109636.
[22] M.R. Hashemi, P.B. Ryzhakov, R. Rossi, Three dimensional modeling of liquid droplet spreading on solid surface: An enriched finite element/level-set approach, J. Comput. Phys. 442 (2021), 110480, https://doi.org/10.1016/j.jcp.2021.110480.
[23] A. Russo, M. Icardi, M. Elsharkawy, D. Ceglia, P. Asinari, C.M. Megaridis, Numerical simulation of droplet impact on wettability-patterned surfaces, Phys. Rev. Fluids 5 (2020) 1–22, https://doi.org/10.1103/PhysRevFluids.5.074002.
[24] D. Seksinsky, J.S. Marshall, Droplet impingement on a surface at low reynolds numbers, J. Fluids Eng. Trans. ASME 143 (2021) 1–16, https://doi.org/10.1115/1.4048289.
[25] X. Shang, Z. Luo, E.Y. Gatapova, O.A. Kabov, B. Bai, GNBC-based front-tracking method for the three-dimensional simulation of droplet motion on a solid surface, Comput. Fluids 172 (2018) 181–195, https://doi.org/10.1016/j.compfluid.2018.06.021.
[26] M. Muradoglu, S. Tasoglu, A front-tracking method for computational modeling of impact and spreading of viscous droplets on solid walls, Comput. Fluids 39 (2010) 615–625, https://doi.org/10.1016/j.compfluid.2009.10.009.
[27] A. Shahmardi, M.E. Rosti, O. Tammisola, L. Brandt, A fully Eulerian hybrid immersed boundary-phase field model for contact line dynamics on complex geometries, J. Comput. Phys. 443 (2021), 110468, https://doi.org/10.1016/j.jcp.2021.110468.
[28] H.R. Liu, C.Y. Zhang, P. Gao, X.Y. Lu, H. Ding, On the maximal spreading of impacting compound drops, J. Fluid Mech. 854 (2018) R6, https://doi.org/10.1017/jfm.2018.702.
[29] S. Al Sofyani, I.D. Marinescu, Analytical modeling of the thermal aspects of metalworking fluids in the milling process, Int. J. Adv. Manuf. Technol. 92 (2017) 3953–3966, https://doi.org/10.1007/s00170-017-0429-4.
[30] J.P. Byers. Metalworking Fluids, second edition, CRC Press, 2006.
[31] M.N. Sharif, S. Pervaiz, I. Deiab, Potential of alternative lubrication strategies for metal cutting processes: a review, Int. J. Adv. Manuf. Technol. (2017), https://doi.org/10.1007/s00170-016-9298-5.
[32] B. Guimarães, C.M. Fernandes, D. Figueiredo, M.F. Cerqueira, O. Carvalho, F. S. Silva, G. Miranda, A novel approach to reduce in-service temperature in WC-Co cutting tools, Ceram. Int. 46 (2020) 3002–3008, https://doi.org/10.1016/j.ceramint.2019.09.299.
[33] C.M. Fernandes, A.M.R. Senos, Cemented carbide phase diagrams: a review, Int. J. Refract. Met. Hard Mater. 29 (2011) 405–418, https://doi.org/10.1016/j.ijrmhm.2011.02.004.
[34] B. Guimarães, D. Figueiredo, C.M. Fernandes, F.S. Silva, G. Miranda, O. Carvalho, Laser machining of WC-Co green compacts for cutting tools manufacturing, Int. J. Refract. Met. Hard Mater. 81 (2019) 316–324, https://doi.org/10.1016/j.ijrmhm.2019.03.018.
[35] Y. Chen, J. Wang, M. Chen, Enhancing the machining performance by cutting tool surface modifications: a focused review, Mach. Sci. Technol. 23 (2019) 477–509, https://doi.org/10.1080/10910344.2019.1575412.
[36] X. Wang, C. Li, Y. Zhang, W. Ding, M. Yang, T. Gao, H. Cao, X. Xu, D. Wang, Z. Said, S. Debnath, M. Jamil, H.M. Ali, Vegetable oil-based nanofluid minimum quantity lubrication turning: academic review and perspectives, J. Manuf. Process. 59 (2020) 76–97, https://doi.org/10.1016/j.jmapro.2020.09.044.
[37] Q. Yin, C. Li, L. Dong, X. Bai, Y. Zhang, M. Yang, D. Jia, R. Li, Z. Liu, Effects of physicochemical properties of different base oils on friction coefficient and surface roughness in MQL milling AISI 1045, Int. J. Precis. Eng. Manuf. Green. Technol. 8 (2021) 1629–1647, https://doi.org/10.1007/s40684-021-00318-7.
[38] X. Wang, C. Li, Y. Zhang, Z. Said, S. Debnath, S. Sharma, M. Yang, T. Gao, Influence of texture shape and arrangement on nanofluid minimum quantity lubrication turning, Int. J. Adv. Manuf. Technol. (2021), https://doi.org/10.1007/s00170-021-08235-4.
[39] J. Hu, R. Jia, K. Wan, X. Xiong, Simulation of Droplet Impingement on a Solid Surface by the Level Set Method, in: 2014 COMSOL Bost. Conf., 2014.
[40] J.C. Crittenden, R. Rhodes Trussell, D.W. Hand, K.J. Howe, G. Tchobanoglous. Appendix C: Physical Properties of Water, in: Water Treat. Princ. Des, third edition, John Wiley & Sons, 2012, pp. 1861–1862.
[41] Y.A. Cengel. Appendix 1 - Property Tables and Charts (SI units), in: Heat Transf. A Prat. Approach, second edition, McGraw - Hill, 2002, p. 884.
[42] G. Kwak, D.W. Lee, I.S. Kang, K. Yong, A study on the dynamic behaviors of water droplets impacting nanostructured surfaces, AIP Adv. 1 (2011), 042139, https://doi.org/10.1063/1.3662046.
[43] X. Hao, H. Li, Y. Yang, S. Xiao, X. Song, L. Li, Experiment on cutting performance of textured cemented carbide tools with various wettability levels, Int. J. Adv. Manuf. Technol. 103 (2019) 757–768, https://doi.org/10.1007/s00170-019-03471-1.
[44] S. Lin, B. Zhao, S. Zou, J. Guo, Z. Wei, L. Chen, Impact of viscous droplets on different wettable surfaces: Impact phenomena, the maximum spreading factor, spreading time and post-impact oscillation, J. Colloid Interface Sci. 516 (2018) 86–97, https://doi.org/10.1016/j.jcis.2017.12.086.
[45] H. Ding, P.D.M. Spelt, Inertial effects in droplet spreading: a comparison between diffuse-interface and level-set simulations, J. Fluid Mech. 576 (2007) 287–296, https://doi.org/10.1017/S0022112007004910.

[46] H. Ding, E.Q. Li, F.H. Zhang, Y. Sui, P.D.M. Spelt, S.T. Thoroddsen, Propagation of capillary waves and ejection of small droplets in rapid droplet spreading, J. Fluid Mech. 697 (2012) 92–114, https://doi.org/10.1017/jfm.2012.49.
[47] A. Cetiner, B. Evren, M. Budakli, M. Arik, A. Ozbek, Spreading behavior of droplets impacting over substrates with varying surface topographies, Colloids Surf. A Physicochem. Eng. Asp. 606 (2020), 125385, https://doi.org/10.1016/j.colsurfa.2020.125385.
[48] B. Guimarães, C.M. Fernandes, D. Figueiredo, O. Carvalho, F.S. Silva, G. Miranda, Effect of laser surface texturing on the wettability of WC-Co cutting tools, Int. J. Adv. Manuf. Technol. 111 (2020) 1991–1999, https://doi.org/10.1007/s00170-020-06155-3.
[49] Y. Zhang, C. Li, M. Yang, D. Jia, Y. Wang, B. Li, Y. Hou, N. Zhang, Q. Wu, Experimental evaluation of cooling performance by friction coefficient and specific friction energy in nanofluid minimum quantity lubrication grinding with different types of vegetable oil, J. Clean. Prod. 139 (2016) 685–705, https://doi.org/10.1016/j.jclepro.2016.08.073.